Check for updates

View Article Online

View Journal

Nanoscale

Accepted Manuscript

Volume 10
Number 4
28 January 2018
Pages 1549-2172

Nanoscale

rsc.li/nanoscale

ISSN 2040-3372

PAPER
Shuping Xu, Chongyang Liang et al.
Organelle-targeting surface-enhanced Raman scattering
(SERS) nanosensors for subcellular pH sensing

ROYAL SOCIETY
OF CHEMISTRY

NCNST

This is an Accepted Manuscript, which has been through the Royal Society of Chemistry peer review process and has been accepted for publication.

Accepted Manuscripts are published online shortly after acceptance, before technical editing, formatting and proof reading. Using this free service, authors can make their results available to the community, in citable form, before we publish the edited article. We will replace this Accepted Manuscript with the edited and formatted Advance Article as soon as it is available.

You can find more information about Accepted Manuscripts in the Information for Authors.

Please note that technical editing may introduce minor changes to the text and/or graphics, which may alter content. The journal's standard Terms & Conditions and the Ethical guidelines still apply. In no event shall the Royal Society of Chemistry be held responsible for any errors or omissions in this Accepted Manuscript or any consequences arising from the use of any information it contains.

ROYAL SOCIETY
OF CHEMISTRY

rsc.li/nanoscale

ARTICLE

Magneto-optical hyperthermia agents based on probiotic bacteria loaded with magnetic and gold nanoparticles

Víctor Garcés,[a] Ana González,[a] Natividad Gálvez,[a] José M. Delgado-López,[a] Jose J. Calvino,[b] Susana Trasobares,[b] Yilian Fernández-Afonso,[c] Lucía Gutiérrez,*[c] and José M. Dominguez-Vera,*[a]

Probiotic bacteria were used as carriers of metallic nanoparticles to develop innovative oral agents for hyperthermia cancer therapy. Two synthetic strategies were used to produce the different therapeutic agents. First, the probiotic bacterium *Lactobacillus fermentum* was simultaneously loaded with magnetic (MNPs) and gold nanoparticles (AuNPs) of different morphologies to produce AuNP+MNP-bacteria systems with both types of nanoparticles arranged in the same layer of bacterial exopolysaccharides (EPS). In the second approach, the probiotic was first loaded with AuNP to form AuNP-bacteria and subsequently loaded with MNP-EPS to yield AuNP-bacteria-EPS-MNP with the MNP and AuNP arranged in two different EPS layers. This second strategy has never been reported and exploits the presence of EPS–EPS recognition which allows the layer-by-layer formation of structures on the bacteria external wall. The AuNP+MNP-bacteria and AuNP-bacteria-EPS-MNP samples were characterized by scanning (SEM) and transmission electron microscopy (TEM), and UV-vis spectroscopy. The potential of these two heterobimetallic systems as magnetic hyperthermia or photothermal therapy agents was assessed, validating their capacity to produce heat either during exposure to an alternating magnetic field or a near-infrared laser light. The probiotic *Lactobacillus fermentum* has already been proposed as an oral drug carrier, able to overcome the stomach medium and deliver drugs to the intestines, and it is actually marketed as an oral supplement to reinforce the gut microbiota, thus, our results open the way for the development of novel therapeutic strategies using these new heterobimetallic AuNP/MNP-bacteria systems in the frame of gastric diseases, using them, for example, as oral agents for cancer treatment with magnetic hyperthermia and photothermal therapy.

1. Introduction

Nanomedicine is increasing the number of possibilities for cancer treatment.[1] One of these new treatment approaches relies on the use of metal nanoparticles, with exceptional optical and magnetic properties.[2,3] In particular, gold nanoparticles (AuNPs) and superparamagnetic maghemite/magnetite nanoparticles (MNPs) are being studied in the frame of hyperthermia treatments applied to tumors.[4,5] Hyperthermia involves killing cells by heating them to temperatures higher than those which normally occur in the body, typically around 40–50 °C.[6] Heating small areas of the tumor causes cancer cell death by denaturing their proteins and damaging their membranes.[7,8] This local temperature increase can be achieved with nanomaterials acting as hyperthermia

agents, converting different forms of energy into heat. In particular, the two main energy sources being used to generate heat with nanoparticles are near-infrared (NIR) laser lights, for photothermal therapy,[9] and alternating magnetic fields for magnetic hyperthermia.[10]

In the frame of photothermal therapy, AuNPs have been widely studied.[11] Their surface plasmon resonance (SPR) is responsible for the absorption of incident light (visible to NIR range) and subsequent heat generation.[12] The SPR absorption wavelength strongly depends on the size, shape and aggregation of the AuNPs.[13] In clinical practice, AuNPs with SPR in the NIR range are especially interesting because NIR wavelengths penetrate much deeper inside the body than other wavelenghts.[14,15] Examples of NIR-absorbing AuNPs include anisotropically shaped AuNPs, e.g., rods and prisms, and some aggregates.[16]

a. *Departamento de Química Inorgánica and Instituto de Biotecnología, Universidad de Granada, 18071 Granada, Spain; E-mail: josema@ugr.es.*
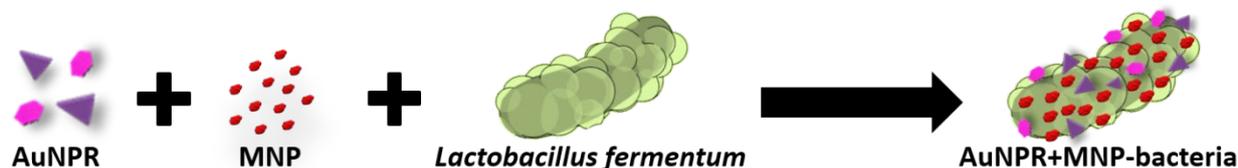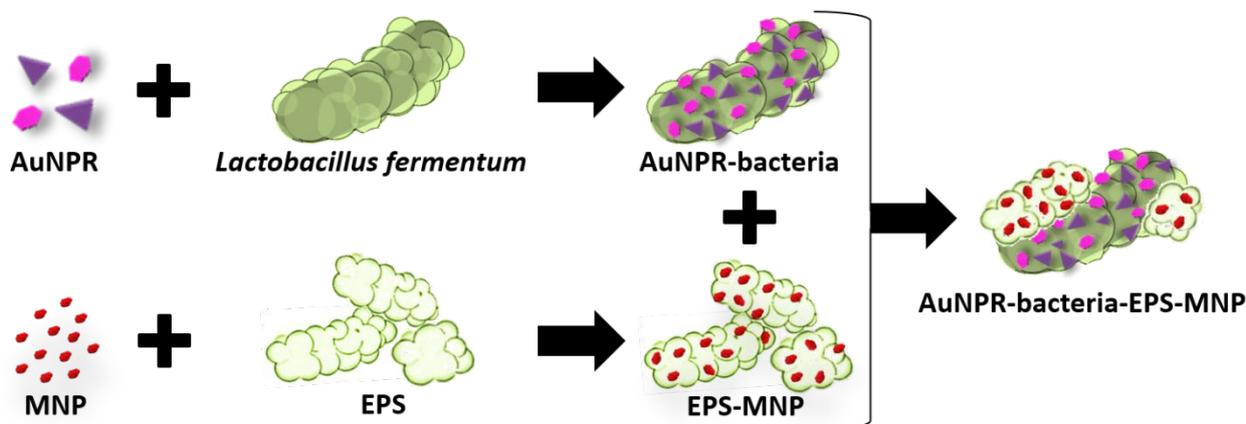b. *Departamento Ciencia de Materiales e Ingeniería Metalúrgica y Química Inorgánica, Universidad de Cádiz, 11510 Cádiz, Spain.*
c. *Departamento de Química Analítica, Instituto de Nanociencia y Materiales de Aragón (INMA), CSIC- Universidad de Zaragoza and CIBER-BBN, 50018 Zaragoza, Spain; E-mail: lu@unizar.es.*

Nanoscale Accepted Manuscript

ARTICLE

A) One-pot synthesis

AuNPR + MNP + *Lactobacillus fermentum* → AuNPR+MNP-bacteria

B) Layer-by-layer synthesis

AuNPR + *Lactobacillus fermentum* → AuNPR-bacteria

MNP + EPS → EPS-MNP

{ AuNPR-bacteria-EPS-MNP }

Scheme 1. Gold nanoprisms (AuNPR) and magnetic nanoparticles (MNP) were incorporated onto the surface of the probiotic bacteria *Lactobacillus fermentum*, either directly (AuNPR+MNP-bacteria) or through a layer-by-layer strategy (AuNPR-EPS-MNP).

On the other hand, in the frame of magnetic hyperthermia, iron oxide MNPs are the main materials being studied for cancer therapies.[16–18] MNPs exposed to alternating magnetic fields release energy to the surroundings via heat transfer. The main mechanisms responsible of this heat production are hysteresis losses and Néel and Brown relaxation processes.[19] The MNP's potential to produce heat can be assessed by measuring its specific absorption rate (SAR), which is related to the energy absorbed per unit mass of nanoparticle.[20] This parameter depends on nanoparticle size, shape and composition, as well as on the frequency (f) and amplitude (H) of the magnetic field.[21–23] Interestingly, in the past few years, the use of MNPs as sources of heat under the exposure to a NIR light has started to be explored too.[24]

Most nanoparticles studied as hyperthermia therapy agents require parenteral administration. This is primarily because therapeutics administered orally have to overcome the harsh environment of the stomach, where nanoparticles usually suffer degradation, limiting the oral administration route possibility.[25] In this scenario, the development of therapeutic agents able to protect the particles in the stomach, would open their use as oral administered agents in the frame of gastrointestinal treatments. One of the possible ways to protect the particles would be the use of probiotic bacteria.

We have previously reported that probiotic bacteria can be used to deliver magnetic nanoparticles to the intestines. In fact, after loading *Lactobacillus fermentum* (Lf), a probiotic marketed as oral supplement that reinforces the gut microbiota, with MNPs and administering it orally to rats, the bacteria were able to transport the MNPs safely through the stomach into the intestines.[26–28] Furthermore, we have also shown that spherical gold nanoparticles can be incorporated in the exopolysaccharide (EPS) layer surrounding the bacterial wall.[29]

In this work, we have gone one step forward, developing two new strategies for the incorporation of both AuNPs and MNPs on the surface of Lf. In the first strategy, both types of nanoparticles were located at the native bacterial EPS layer, whereas in the second one, they were incorporated in two different EPS layers, the native bacterial EPS layer and a second layer incorporated in a separate step afterwards. These new approaches resulted in a library of AuNP/MNP-bacteria systems, with gold nanoparticles of different morphologies and different AuNP/MNP distributions (Scheme 1). We then studied the heterobimetallic systems' potential as heating agents in magnetic hyperthermia and photothermal therapy.

Nanoscale Accepted Manuscript

2. Experimental

2.1 Materials

All reagents were purchased from Sigma Aldrich.

2.2 Synthesis of maghemite nanoparticles

Maghemite nanoparticles (MNP) were synthesized following Massart's method with the co-precipitation of Fe(II) and Fe(III) salts ($FeCl_2$ and $FeCl_3$) in a stoichiometry of 0.5.[30] Adjusting the pH to 11 with 3 M sodium hydroxide (NaOH) and the ionic strength with 1 M sodium nitrate ($NaNO_3$), produced magnetite nanoparticles with an average size of 10 nm. After oxidizing the magnetite to maghemite with 1 M perchloric acid ($HClO_4$) and magnetic decantation, we obtained a colloid of maghemite nanoparticles stable at pH 2.5. A complete characterization of the maghemite particles was performed including Transmission electron microscopy (TEM) and Dynamic Light Scattering (DLS) size distributions, zeta potential measurements and X-ray Diffraction (XRD) analysis (Figures SI1 and SI2 of the Supporting information). Furthermore, the stability of the particles at low pH was verified by TEM, DLS, zeta potential and XDR measurements at two different time points, immediately after synthesis and one year later verifying that their remained unchanged during that time (see Supporting information).

2.3 Synthesis of gold nanorods

We used a seed-mediated method to prepare gold nanorods (AuNR).[31] Solutions of 1 mM $HAuCl_4 \cdot 3H_2O$, 8 mM silver nitrate ($AgNO_3$), 78.8 mM ascorbic acid ($C_6H_8O_6$) and 10 mM sodium borohydride ($NaBH_4$) were prepared at room temperature. The $NaBH_4$ solution was ice-cooled after preparation. Solutions of 0.2 M cetyltrimethylammonium bromide (CTAB) and 92 mM (11-mercaptoundecyl)-N,N,N-trimethylammonium bromide (MUTAB) were prepared by heating at 50 °C, stirring until dissolved and then cooling to room temperature. All the solutions were prepared in Milli-Q ultrapure water. Gold seed synthesis was as follows: 5 mL of 0.2 M CTAB, 2.5 mL of 1 mM $HAuCl_4$ and 0.6 mL of ice-cold 10 mM $NaBH_4$ were mixed and stirred for 2 min at 25 °C. When seeds formed, the solution changed from yellow to a light brown color. AuNR synthesis was as follows: 5 mL of 0.2 M CTAB were placed in a flask previously heated in an oil bath at 30 °C and under stirring at 180 rpm. 5 mL of 1 mM HAuCl4, 70 μL of 78.8 mM ascorbic acid and 100 μL of 8 mM $AgNO_3$ were added in that order to the CTAB solution. The mixture was completed with 160 μL of the seed solution. The final mixture was stirred at 180 rpm and 30 °C for 48 h. Due to CTAB's antibacterial activity,[32] it was replaced by MUTAB. To this end, gold nanoparticles with CTAB as cap ligand were collected twice by high-speed centrifugation at 13,000 rpm for 10 min, dissolved in 1 mL of Milli-Q ultrapure water and 1 mL of 92 mM MUTAB, and stirred gently. Forty-eight hours later, gold nanoparticles were collected again by high-speed centrifugation at 13,000 rpm for 10 min and the pellet dissolved in 1 mL of Milli-Q ultrapure water. The AuNR were characterized by UV-vis spectroscopy (using a Thermo Spectronic Unicam UV 300

spectrophotometer) and TEM (Figure SI3 of the Supporting information).

2.4 Synthesis of gold nanoprisms

Gold nanoprisms (AuNPR) were synthesized following a previously reported protocol.[33] 100 mL of $HAuCl_4$ 2 mM and 120 mL of fresh sodium thiosulfate ($Na_2S_2O_3$) 0.5 mM, both prepared in Milli-Q ultrapure water, were mixed and stirred gently at 15 °C. After 9 min ("seed" formation) an extra 50 mL of fresh $Na_2S_2O_3$ 0.5 mM was added. Growth mixture was left overnight at 15 °C under mild stirring conditions. The AuNPR were characterized by UV-vis spectroscopy (using a Thermo Spectronic Unicam UV 300 spectrophotometer), TEM and DLS. Photothermal capacity of AuNPR was also assessed (Figure SI4 of the Supporting information).

2.5 *Lactobacillus fermentum* culture

Lactobacillus fermentum, supplied by Biosearch S.A., were grown in a synthetic bacterial growth medium at 37 °C on an orbital shaker for 24 h and with an initial concentration of 1 mg bacteria in 1 mL of medium. The synthetic growth medium consisted of (g·L^{-1}) sodium phosphate dibasic (Na_2HPO_4) – 5.0, monopotassium phosphate (KH_2PO_4) – 6.0, tris-ammonium citrate ($C_6H_{14}N_2O_7$) – 2.0, sucrose ($C_{12}H_{22}O_{11}$) – 50.0, magnesium sulfate ($MgSO_4$) – 1.0 and trace elements solution – 10 mL (consisting of (g·L-1): manganese sulfate ($MnSO_4$) – 2.0, cobalt chloride ($CoCl_2$) – 1.0, zinc chloride ($ZnCl_2$) – 1.0 dissolved in 0.1 M hydrochloric acid (HCl) solution). The medium had an initial pH of 6.7 and was sterilized at 121 °C.

2.6 Grafting maghemite nanoparticles to the bacteria

To prepare bacteria labeled with maghemite nanoparticles (MNP-bacteria), 10 mL of bacteria culture were centrifuged at 3000 g for 5 min and washed with distilled water. Then, an acidic solution (pH 2) of MNPs (66.6 μL, 0.95 M) was added to the bacteria in an ice bath and mixed. The solution was diluted to 1 mL with distilled water. MNP–bacteria were collected at 100 g , 20 min. MNP-bacteria characterization was carried out by TEM as reported previously.[34] The stability of this type of system in conditions similar to those of the stomach was verified in the past and the results were patented.[28]

2.7 Grafting gold nanoparticles to the bacteria

Two different 10 mL aliquots of a Lf culture were collected and centrifugated at 3000 g for 10 min. 2 mL of each AuNR or AuNPR colloids were added to each bacterial pellet. AuNR-bacteria and AuNPR-bacteria were collected at 100 g for 20 min and characterized by UV-vis spectroscopy (using a Thermo Spectronic Unicam UV 300 spectrophotometer), TEM, high-angle annular dark-field scanning transmission electron microscopy (HAADF-STEM) and energy-dispersive X-ray spectroscopy (EDX) as previously reported.[35]

Nanoscale Accepted Manuscript

2.8 Simultaneous grafting of MNP and AuNPR to the bacteria

To incorporate both MNP and AuNPR onto the bacterial surface, 33.3 µL of 0.95 M MNP were mixed with 2 mL of AuNPR colloidal solution and stirred until the mixture was homogenized. A 10 mL aliquot of a Lf culture was collected and centrifuged at 3000 g for 10 min. Then, the MNP+AuNPR mixture was added to bacteria. AuNPR+MNP-bacteria were collected at 100 g for 20 min and characterized by UV-vis spectroscopy (using a Thermo Spectronic Unicam UV 300 spectrophotometer) and TEM.

2.9 Isolating EPS layer from *L. fermentum*

The bacteria were removed by centrifugation at 3000 g for 10 min. The supernatant was filtered using a EMD Millipore Steritop™ Sterile Vacuum Bottle-Top Filter. Ice-cold ethanol (2 vol) was added to the cell-free supernatant (1 vol) under continuous stirring, then stored overnight in a refrigerator to promote precipitation. The alcoholic supernatant was centrifuged at 22,000 g for 35 min and the precipitated EPS were washed with acetone and centrifuged once again. The solid obtained was dissolved in distilled water (100 mL), and dialyzed against distilled water for 24 h (MWCO 12,000 to 14,000 D). The dialyzed solution was lyophilized.

2.10 Deposition of MNP onto EPS layers

A 10 mg mL^{-1} solution of EPS in water was adjusted to pH 2 using 1 M HCl. The EPS solution was heated at 80 °C for 24 h under continuous stirring at 200 rpm. The solution was cooled to room temperature. Each EPS-MNP sample consisted on 130 µL of a 1 to 10 times diluted MNP solution added to 650 µL of an EPS pH 2 solution.

2.11 Deposition of EPS-MNP over AuNPR-bacteria

An EPS-MNP sample (see 2.10) was added to an AuNPR-bacteria sample (see 2.7) and incubated at 37 °C for 3 h. The resulting AuNPR-bacteria-EPS-MNP systems were centrifuged at 100 g for 30 min and the pellets diluted in 500 µL of acidic water (pH 2) before characterizing them by TEM.

2.12 Elemental analysis

Freeze-dried AuNP+MNP-bacteria systems were weighed and acid digested for elemental analysis by adding aqua regia (HCl:HNO$_3$, 3:1 v/v) and heating up to 60 °C for 30 min using a hot block. After that, the samples were allowed to cool down to room temperature and 30 % H$_2$O$_2$ (w/v) was added and heated up to 95 °C for 1 h. Inductively coupled Plasma Optical Emission Spectroscopy (ICP-OES) in a Perkin Elmer Optima 2100 DV was used to determine the gold and iron concentrations. The amounts of gold and iron per sample are shown in Table SI1 of the Supporting Information.

2.13 Transmission electron microscopy

To prepare TEM samples, a drop of the sample was placed on a carbon-coated Cu grid (200 mesh) designed specifically for TEM. The grid was blotted with filter paper. Electron micrographs were taken with a LIBRA 120 PLUS microscope (Carl Zeiss SMT) operating at 120 keV and a Philips CM-20 HR analytical electron microscope operating at 200 keV. Nanoanalytical information for the samples were obtained using a FEI Titan Cubed Themis 60-300 microscope operating at 300 kV. The Double Aberration-Corrected Scanning Transmission Electron microscope (STEM) was equipped with a Super X-G2 X-ray energy-dispersive spectrometer, thus providing a tool to simultaneously combine spectroscopy and image signals. The large area views of the samples were recorded using the scanning High Angle Annular Dark Field detector.

2.14 Photothermal therapy properties characterization

The photothermal conversion was studied by measuring the temperature variation of the sample (450 µL) while it was irradiated using a laser (Laser Quantum, mpc6000/Ventus 1064) of λ = 1064 nm using a power of 1 W. The suspension was placed into a quartz cuvette (2 mm optical path) with magnetic stirring. The suspension temperature was recorded with a T-type thermocouple coupled to a Datalogger USB (TC Direct). The beam spot size was 2.2 mm (beam diameter) resulting in an irradiated sample volume of 0.04 mL. The control sample was Milli-Q water. The SAR ($kW \cdot g_{Au}^{-1}$) was calculated using Equation (1).[24]

$$SAR = \frac{C_{p_{H_2O}} \times m_{H2O}}{m_{NPs}} \times \frac{dT}{dt} \quad [kW \cdot g_{Au}^{-1}] \quad (1)$$

Where $C_{p_{H_2O}}$ is the specific heat capacity of water (4.186 J·g^{-1}·K^{-1}), m_{H2O} is the mass of water (g), m_{NPs} is the mass of Au (g) corresponding to NPs in the irradiated volume (considering the spot size and the cuvette length), and (dT/dt) is the initial slope of the heating curve (first 30 sec).

2.15 Magnetic hyperthermia properties characterization

Magnetic hyperthermia measurements were performed using a commercial equipment (D5 Series from nB nanoScale Biomagnetics). The temperature was recorded using a fiber optic sensor. A volume (500 µL) of the samples in suspension at 0.5 mg$_{Fe}$/mL was placed into a glass vial located at the center of the magnetic induction coil inside an isolating holder. The temperature increase over time was recorded at 763.4 kHz and 360 Gauss. The SAR ($W \cdot g_{Fe}^{-1}$) was calculated using Equation (1) were m_{NPs} is the iron mass (g) corresponding to magnetic nanoparticles in the sample.

3. Results and Discussion
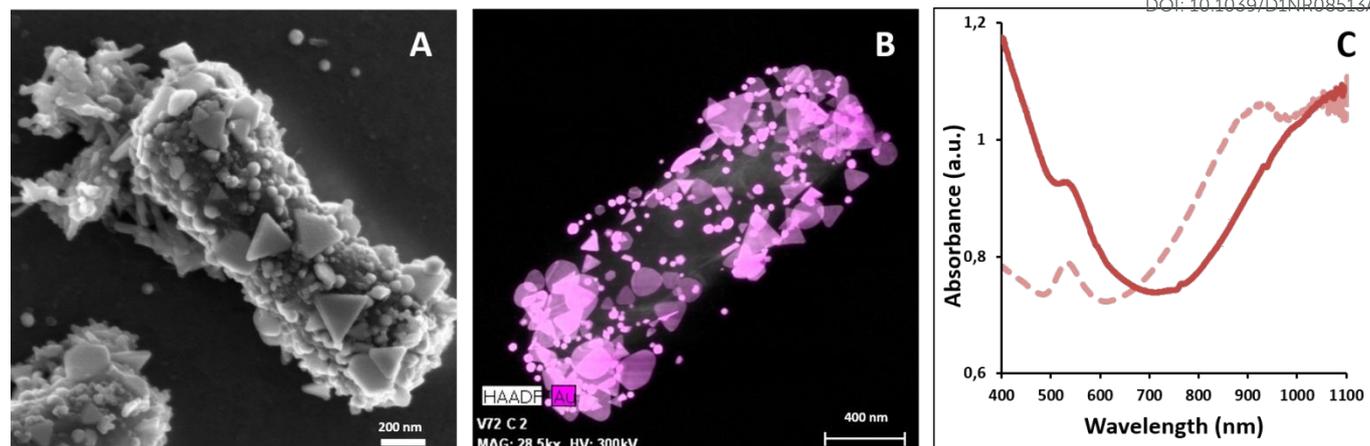
Figure 1. A) SEM image of the AuNPR-bacteria. B) HAADF-STEM merged with EDX compositional analysis of the AuNPR-bacteria (gold in pink). C) UV-vis spectra of AuNPRs (dashed line) and AuNPR-bacteria (solid line).

3.1 AuNPR-bacteria and AuNR-bacteria

Gold nanoprisms (AuNPR) and gold nanorods (AuNR) were prepared as reported elsewhere[31,33] and incubated separately with Lf. The resulting AuNPR- and AuNR-bacteria samples were studied using HAADF-STEM and EDX (Figure 1). Aggregated nanoprisms and some smaller spherical gold nanoparticles were found attached to the native EPS of the probiotic bacterium, with a fairly homogeneous distribution of the particles around the bacteria surface. The analysis of the absorbance of this system revealed that the AuNPR-bacteria absorbance maxima shifted to lower energies (around 1100 nm) compared to isolated nanoparticles (935 nm), probably caused by the local aggregation of the particles on the bacteria surface. Interestingly, the AuNRs adhered to the bacterial EPS layer in a much lower amount than the AuNPRs (Figure SI5 of the Supplementary Information). In such a case, the UV-vis spectrum of the AuNR-bacteria system presented a broad absorption, with no maximum (Figure SI5).

The photothermal conversion efficiency of AuNPR- and AuNR-bacteria was measured during 5 minutes under the exposure to laser irradiation at 1064 nm (Figure 2A). When using a concentration of bacteria of 2 mg/mL, the temperature increase produced by the AuNPR-bacteria system at the final time point was 24 °C. In contrast, the AuNR-bacteria, prepared at the same concentration, induced a 6 °C rise at the same time point. This difference was caused by the higher concentration of gold nanoparticles in the AuNPR-bacteria (20% w/w or 200 mg_{Au}/g_{sample}) compared to the AuNR-bacteria system (3% w/w, 30 mg_{Au}/g_{sample}). Table SI1 shows the amount of gold for these samples. Heating curves were also recorded preparing a sample with the same Au concentration (0.05 mg_{Au}/mL). In such measurement conditions, similar results were obtained for both systems being the SAR of the AuNPR 193 kW/g_{Au} and the SAR of the AuNR-bacteria 190 kW/g_{Au}. Therefore, the loading factor of the bacteria with the AuNPs was a fundamental factor for the heat generation. From the presented results, it was verified that the heating capacity of the AuNPR-bacteria allowed them to be used as a photothermal agents.
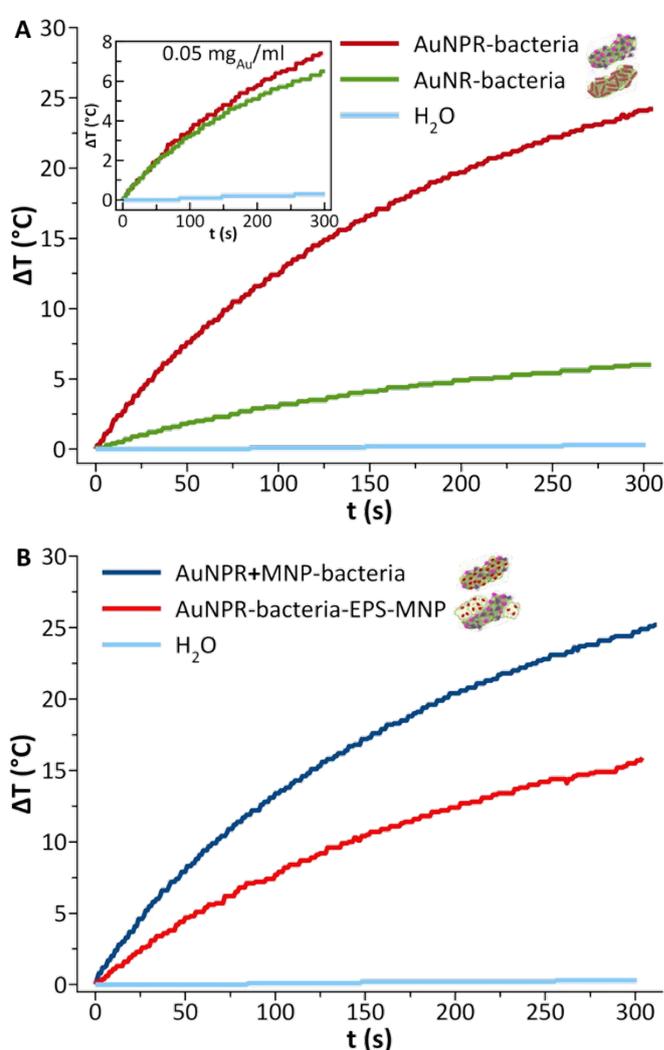

Figure 2. Heating curves obtained after laser irradiation of 2 mg/mL of: A) AuNPR-bacteria and AuNR-bacteria, plus water as a control sample, with inset of measurements of the same diluted sample at 0.05 mg_{Au}/mL; and B) AuNPR+MNP-bacteria and AuNPR-bacteria-EPS-MNP, plus water as a control sample.

3.2 Heterobimetallic probiotic AuNPR+MNP-bacteria and AuNPR-bacteria-EPS-MNP

Bearing in mind the efficient optical heating of the AuNPR-bacteria system, additional modifications were performed to the preparation protocol in order to incorporate a different material with distinct properties. In particular, MNPs were selected as they could be used as heating sources under the exposure to an external alternating magnetic field. We used two different strategies to incorporate both AuNPRs and MNPs on the same bacterium, which gave rise to two different heterobimetallic structures containing both types of nanoparticles.

In the first strategy, AuNPRs and MNPs were mixed and then directly added to Lf. HAADF-STEM in combination with EDX analysis revealed that both AuNPRs and MNPs were incorporated onto the Lf. The MNPs seemed to homogeneously cover the whole native Lf EPS layer, while small gold aggregates were randomly distributed across the same surface. This sample, hereinafter called AuNPR+MNP-bacteria, had an absorbance maximum in the UV-vis spectrum shifted to a lower wavelength (1100 nm) compared to free AuNPRs and close to that of AuNPR-bacteria (Figure 3).
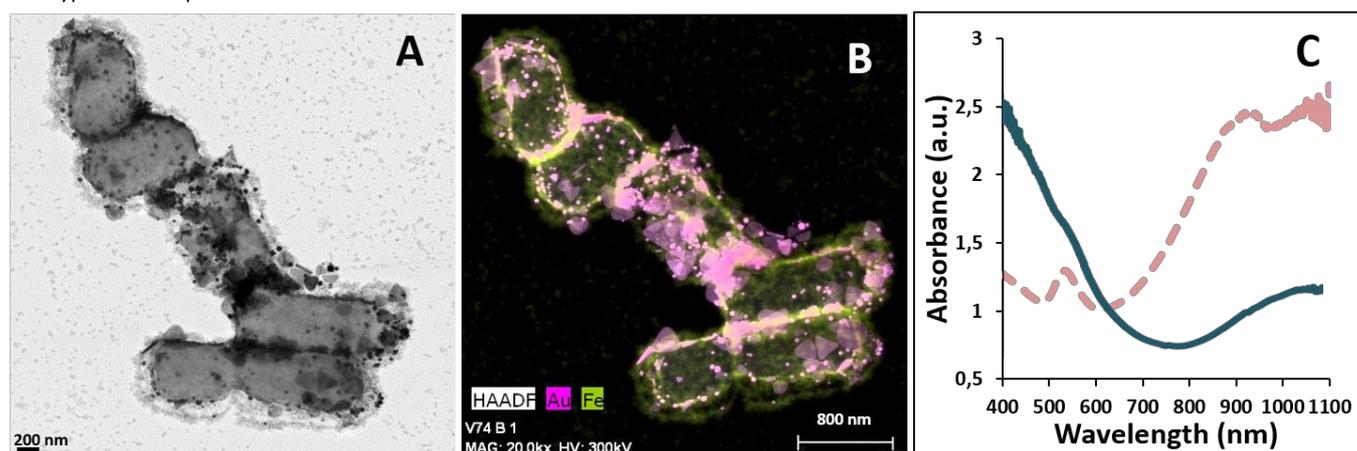
Figure 3. A) TEM image of the AuNPR+MNP-bacteria. B) HAADF-STEM/EDX image of the AuNPR+MNP-bacteria (Au, pink; Fe, green). C) UV-visible spectra of AuNPR+MNP-bacteria (solid line) showing the SPR shift to a lower energy compared to that of the AuNPRs (dashed line).
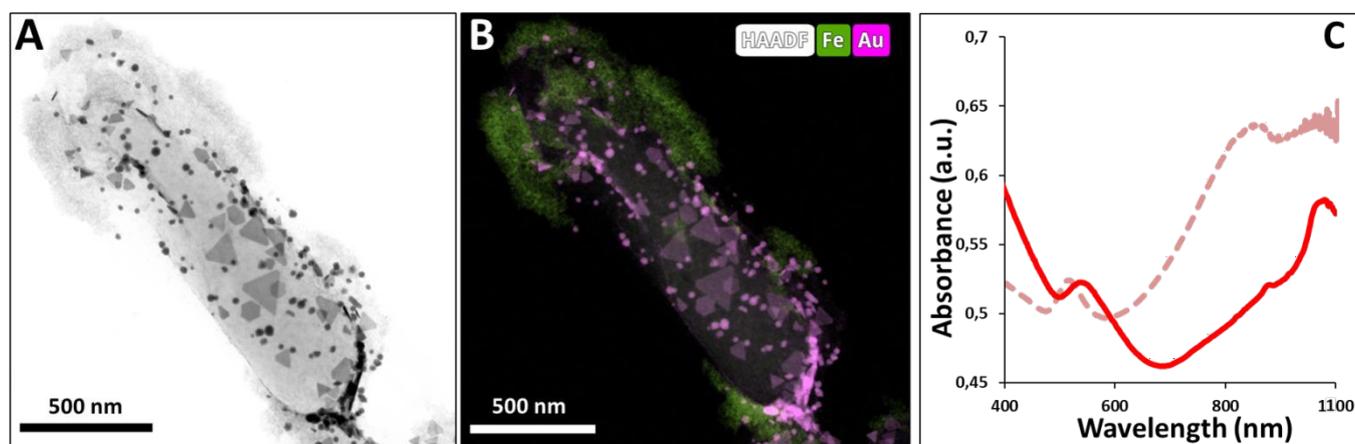
Figure 4. A) TEM image of AuNPR-bacteria-EPS-MNP. B) HAADF-STEM combined with EDX compositional analysis images of AuNPR-bacteria-EPS-MNP (iron in green and gold in pink). The different types of nanoparticles formed discernable layers in this nanosystem. C) UV-visible spectra of AuNPR-bacteria-EPS-MNP (solid line) showing the SPR shift to a lower energy compared to that of the free AuNPRs (dashed line)

For the second strategy, AuNPRs and MNPs were incorporated onto bacteria in a layer-by-layer approach. First, isolated AuNPR-bacteria were prepared and then an additional layer prepared by the combination of EPS and MNPs was added. EPS-MNPs were prepared by isolating the EPS from Lf and then loading it with MNPs following protocols previously described.[12] The main aim was to make use of the EPS-EPS recognition mechanism in which the native EPS of the AuNPR-bacteria couples with the MNP-loaded EPS, giving rise to a bilayer structure. This system was called AuNPR-bacteria-

EPS-MNP, with the metallic blocks (AuNPR and MNP) located in two different EPS layers.

Analysis of AuNPR-bacteria-EPS-MNP by HAADF-STEM-EDX (Figure 4) confirmed that the EPS-MNPs were adhered to the AuNPR-bacteria. In this case, the EPS-MNP layer only covered partially the surface of the AuNPR-bacteria (see Figure SI6 for a more detailed TEM analysis of AuNPR-bacteria-EPS-MNP). When analysing the heating properties of this layer-by-layer system, AuNPR-bacteria-EPS-MNP exhibited an absorbance band in the UV-vis spectrum at around 1100 nm, similar to the observed for the AuNPR-bacteria

system (Figure 4). The amount of gold and iron in AuNPR+MNP-bacteria and AuNPR-bacteria-EPS-MNP can be found in Table SI1.

The heating properties of both heterobimetallic samples - AuNPR+MNP-bacteria (produced in a one-pot synthesis) and AuNPR-bacteria-EPS-MNP (produced via layer-by-layer synthesis) - were measured using the same concentration of bacteria (2 mg_{sample}/mL) during 5 minutes of exposure to laser irradiation (1064 nm). A temperature increase of 25°C and 19 °C was recorded for the AuNPR+MNP-bacteria and AuNPR-bacteria-EPS-MNP, respectively. Such temperature increase was of the same order as that of AuNPR-bacteria (24 °C). The SAR analysis of these samples containing two metals that heat at a different rate was not a straightforward calculation. Although it could be assumed that most of the heat was produced by the AuNPR, the UV-vis spectrum of MNP-bacteria showed non-negligible absorptions at 1064 nm (Figure SI7). However, the heat produced by MNP-bacteria was 3.4 times lower than that of the heterobimetallic systems after 5-minute irradiation (Figure SI7). Nevertheless, using the mass of both metals for the SAR analysis would underestimate the heat produced by the AuNPR. In this work, as an approach to obtain a parameter that describes our systems SAR was calculated using only the Au mass, resulting in SAR values of 125.4 and 87.4 kW/g_{Au}, for the AuNPR+MNP-bacteria and AuNPR-bacteria-EPS-MNP respectively, lower than that of AuNPR-bacteria (193 kW/g_{Au}). In any case, the increase of temperature produced by AuNPR+MNP-bacteria and AuNPR-bacteria-EPS-MNP indicated that these systems have a potential use in photothermal therapy.

Finally, as AuNPR+MNP-bacteria and AuNPR-bacteria-EPS-MNP contained magnetic nanoparticles that can additionally contribute to generate heat under the exposure to an alternating magnetic field, their heating properties in the frame of magnetic hyperthermia were analysed and compared to that of MNP and MNP-bacteria. Heating curves (Figure 5) were measured after exposing the samples during 5 minutes to a high-frequency alternating magnetic field. The curves showed temperature increases of 2.6, 3, 5 and 7 °C during the measurement time, resulting in SAR values of 80, 117, 185 and 463 W/g_{Fe} for AuNPR-bacteria-EPS-MNP, AuNPR+MNP-bacteria, MNP-bacteria and MNP respectively. Although the increase of temperature was higher for the MNP, it is difficult to compare this system with those including bacteria in their formulations as the nature of the samples is completely different from each other. The higher SAR value of MNP-bacteria with respect to those of heterobimetallic samples could be explained in terms of the greater aggregation of MNPs in MNP-bacteria than in AuNPR+MNP-bacteria and AuNPR-bacteria-EPS-MNP, as found in TEM micrographs (Figure SI8). In any case, although the temperature increases were low, these results pointed out the dual nature of AuNPR+MNP-bacteria and AuNPR-bacteria-EPS-MNP as magnetic hyperthermia and photo-thermal therapy agents.
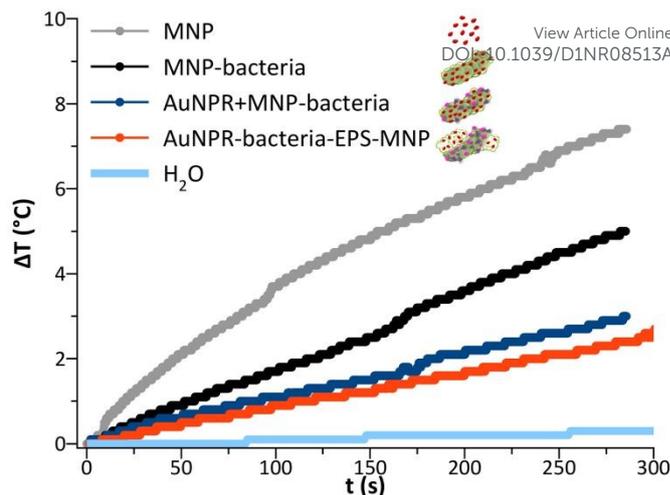
Figure 5. Temperature variation over time for MNP, MNP-bacteria, AuNPR+MNP-bacteria and AuNPR-bacteria-EPS-MNP at 0.5 mgFe/mL after exposing during 5 min the samples to a high-frequency alternating magnetic field. The steps observed in the measurement are a consequence of the temperature probe resolution.

The number of manuscripts describing bacteria as magnetic hyperthermia agents is very limited and most examples focus on the use of magnetotactic bacteria or their magnetosomes.[36] The heating properties of magnetotactic bacteria reported in those studies were apparently better than those of our heterobimetallic bacteria.[37] However, future developments in the frame of magnetotactic bacteria, to improve their heating properties, have important limitations with respect to the heterobimetallic systems that we propose in this work. On one hand, magnetotactic bacteria could not make use of nanoparticles with different magnetic properties,[38] since the formation mechanism of magnetosomes is hardly tuneable.[39] On the other hand, magnetotactic bacteria are difficult to manipulate for the incorporation of an additional hyperthermia agent, such as gold nanoparticles. In this sense, the presented results showed higher temperatures when the heterobimetallic systems were exposed to the NIR light than the AC magnetic field. Besides, it has to be noted that *Lactobacillus fermentum* displays specific properties that make the heterobimetallic bacteria unique drugs to be used as hyperthermia agents of intestinal disseases.[40] In particular, in this system, functional nanoparticles are embedded within the *Lactobacillus fermentum* EPS, which resulted a key aspect to protect the particles when passing through the stomach after oral administration. Furthermore, these bacteria have previously shown their capability to accumulate in specific areas of the intestine.[27,28] Moreover, *Lactobacillus fermentum* was already approved by regulatory agencies and commercialized for therapeutic uses by oral administration,[41] which is extremely helpful to fulfil the gap between the development of new therapeutic systems and the final clinical applications. Therefore, the systems presented in this work would solve the drawback of magnetotactic bacteria as oral hyperthermia agents, by the possible incorporation of different types of nanoparticles that could be adapted to the specific heating properties needed for each application[42] and would open the future

ARTICLE

possibilities to use the heterobimetallic bacteria as therapeutic agents for diseases associated to specific areas of the intestine,[27] in particular, they would be suitable candidates to treat tumours being developed in such areas.

Conclusions

Maghemite and prism gold nanoparticles were incorporated onto the surface of the probiotic bacterium *Lactobacillus fermentum* following two different strategies: a one-pot route and a layer-by-layer approach. The two heterobimetallic systems obtained, AuNPR+MNP-bacteria and AuNPR-bacteria-EPS-MNP presented adequate features to act as dual agents in the frame of magnetic hyperthermia and photothermal therapy. In fact, these materials produced a temperature increase of 19-25 °C when irradiated with a NIR light (1064 nm), and of 2.6-3 °C when exposed to high-frequency alternating magnetic field. This wide range of temperature variation could be used to modulate the heat produced depending on the treatment necessities. The fact that the probiotic *Lactobacillus fermentum* is already in use as an oral supplement that reinforces the gut microbiota, improves its chances to be approved by regulatory agencies as a drug carrier in the future. In addition, this probiotic is able to transport nanoparticles safely through the stomach into the intestines. Therefore, this work encourages further studies of these systems as oral drugs for the treatment of gastrointestinal tumours by bimodal magnetic hyperthermia and photothermal therapy.

Author Contributions

All authors contributed to the design and implementation of the research, to the analysis of the results and to the writing of the manuscript.

Conflicts of interest

There are no conflicts of interest to declare.

Acknowledgements

References

1   G. Chen, I. Roy, C. Yang and P. N. Prasad, *Chem. Rev.*, 2016, **116**, 2826–2885.

2   L. Shang, L. Yang, J. Seiter, M. Heinle, G. Brenner-Weiss, D. Gerthsen and G. U. Nienhaus, *Adv. Mater. Interfaces*, 2014, **1**, 1–10.

3   B. G. A. Ozin, *Precis. Eng.*, 1993, **15**, 206.

4   N.T. Dung, N. T. N. Linh, D. L. Chi, N. T. H. Hoa, N. P. Hung, N. T. Ha, P. H. Nam, N. X. Phuc, L. T. Tam and L. T. Lu, *RSC Adv.*, 2021, **11**, 13458–13465.

5   W. Mekseriwattana, P. Guardia, B. Torres Herrero, J. Martinez de la Fuente, C. Kuhakarn, A. Roig and K. P. Katewongsa, *Nanoscale Adv.*, 2022, DOI: 10.1039/D2NA00015F.

6   J. Kolosnjaj-Tabi, I. Marangon, A. Nicolas-Boluda, A. K. A. Silva and F. Gazeau, *Pharmacol. Res.*, 2017, **126**, 123–137.

7   T. F. Cabada, C. S. L. de Pablo, A. M. Serrano, F. del P. Guerrero, J. J. S. Olmedo and M. R. Gomez, *Int. J. Nanomedicine*, 2012, **7**, 1511–1523.

8   T. Fernández Cabada,PhD thesis, Univ. Politécnica Madrid, 2014.

9   X. Li, Y. Zhang, G.K. Liu, Z. Luo, L. Zhou, Y. Xue and M. Liu, *RSC Adv.*, 2022, **12**, 7635–7651.

10 H. Gavilán, S. K. Avugadda, T. Fernández-Cabada, N. Soni, M. Cassani, B. T. Mai, R. Chantrell and T. Pellegrino, *Chem. Soc. Rev.*, 2021, **50**, 11614–11667.

11 K. Weintraub, *Nature*, 2013, **495**, 4–6.

12 A. González, V. Garcés, L. Sabio, F. Velando, M. López-Haro, N. Gálvez, J. J. Calvino and J. M. Dominguez-Vera, *J. Appl. Phys.*, 2019, **126**, 053101.

13 M. Alrahili, R. Peroor, V. Savchuk, K. McNear and A. Pinchuk, *J. Phys. Chem. C*, 2020, **124**, 4755–4763.

14 Y. Liu, J. Kangas, Y. Wang, K. Khosla, J. Pasek-Allen, A. Saunders, S. Oldenburg and J. Bischof, *Nanoscale*, 2020, **12**, 12346–12356.

15 C. L. Nehl, H. Liao and J. H. Hafner, *Nano Lett.*, 2006, **6**, 683–688.

16 R. Bhattacharya and P. Mukherjee, *Adv. Drug Deliv. Rev.*, 2008, **60**, 1289–1306.

17 X. Huang, P. K. Jain, I. H. El-Sayed and M. A. El-Sayed, *Lasers Med. Sci.*, 2008, **23**, 217–228.

18 R. Das, N. Rinaldi-Montes, J. Alonso, Z. Amghouz, E. Garaio, J. A. García, P. Gorria, J. A. Blanco, M. H. Phan and H. Srikanth, *ACS Appl. Mater. Interfaces*, 2016, **8**, 25162–25169.

19 L. Dykman and N. Khlebtsov, *Chem. Soc. Rev.*, 2012, **41**, 2256–2282.

20 R. A. Frimpong and J. Z. Hilt, *Nanomedicine*, 2010, **5**, 1401–1414.

21 P. Guardia, R. Di Corato, L. Lartigue, C. Wilhelm, A. Espinosa, M. Garcia-Hernandez, F. Gazeau, L. Manna and T. Pellegrino, *ACS Nano*, 2012, **6**, 3080–3091.

22 E. Garaio, J. M. Collantes, J. A. Garcia, F. Plazaola, S. Mornet, F. Couillaud and O. Sandre, *J. Magn. Magn. Mater.*, 2014, **368**, 432–437.

23 J. Kolosnjaj-Tabi, Y. Javed, L. Lartigue, J. Volatron, D. Elgrabli, I. Marangon, G. Pugliese, B. Caron, A. Figuerola, N. Luciani, T. Pellegrino, D. Alloyeau and F. Gazeau, *ACS Nano*, 2015, **9**, 7925–7939.

24 A. Espinosa, J. Reguera, A. Curcio, Á. Muñoz-Noval, C. Kuttner, A. Van de Walle, L. M. Liz-Marzán and C. Wilhelm, *Small*, 2020, **16**, 1–14.

25 R. N. R. Anreddy, *Toxicol. Rep.*, 2018, **5**, 903–904.

26 M. Martín, A. Rodríguez-Nogales, V. Garcés, N. Gálvez, L. Gutiérrez, J. Gálvez, D. Rondón, M. Olivares and J. M. Dominguez-Vera, *Nanoscale*, 2016, **8**, 15041–15047.

27 V. Garcés, A. Rodríguez-Nogales, A. González, N. Gálvez, M. E. Rodríguez-Cabezas, M. L. García-Martin, L. Gutiérrez, D. Rondón, M. Olivares, J. Gálvez and J. M. Dominguez-Vera, *Bioconjug. Chem.*, 2018, **29**, 1785–1791.

28 J.M Dominguez-Vera, N. Galvez, M.A. Martín, F. Carmona, M. Olivares. WO Pat., 206969, 2014.

29 F. Carmona, M. Martín, N. Gálvez and J. M. Dominguez-Vera, *Inorg. Chem.*, 2014, **53**, 8565–8569.

30 R. Massart, *IEEE Trans. Magn.*, 1981, **17**, 1247–1248.

31 B. Nikoobakht and M. A. El-Sayed, *Chem. Mater.*, 2003, **15**, 1957–1962.

32 Y. Jin, J. Deng, J. Liang, C. Shan and M. Tong, *Colloids Surfaces B Biointerfaces*, 2015, **136**, 659–665.

33 B. Pelaz, V. Grazu, A. Ibarra, C. Magen, P. del Pino and J. M. de la Fuente, *Langmuir*, 2012, **28**, 8965–8970.

34 M. Martín, F. Carmona, R. Cuesta, D. Rondón, N. Gálvez and J. M. Domínguez-Vera, *Adv. Funct. Mater.*, 2014, **24**, 3489–3493.

35 V. Garcés, A. González, L. Sabio, C. M. Sánchez-Arévalo, N. Gálvez and J. M. Dominguez-Vera, *Materials*, 2020, **13**, 481.

36 E. Alphandéry, S. Faure, L. Raison, E. Duguet, P. A. Howse and D. A. Bazylinski, *J. Phys. Chem. C*, 2011, **115**, 18–22.

37 D. Gandia, L. Gandarias, I. Rodrigo, J. Robles-García, R. Das, E. Garaio, J. A. García, M-H. Phan, H. Srikanth, I. Orue, J. Alonso, A. Muela and M. L. Fdez-Gubieda, *Small*, 2019, **15**, 1902626.

38 S. Del Sol-Fernández, Y. Portilla-Tundidor, L. Gutiérrez, F. Odio, E. Reguera, F. Barber, and M. P. Morales, *ACS Appl. Mater. Interfaces*, 2019, **11**, 26648–26663.

39 L. Yan, S. Zhang, P.Chen, H. Liu, H. Yin and H. Li, *Microbiol. Res.*, 2012, **167**, 507–519.

40 W. Hao, R. Cha, M. Wang, P. Zhang and X. Jiang, *Nanoscale Horiz.*, 2022, **7**, 6–30.

41 J. Maldonado, F. Cañabate, L. Sempere, F. Vela, A. R. Sánchez, E. Narbona, E. López-Huertas, A. Geerlings, A. D. Valero, M. Olivares and F. Lara-Villoslada, JPGN, 2012, **54**, 55–61.

42 C. Caro, F. Gámez, P. Quaresma, J. M. Páez-Muñoz, A. Domínguez, J. R. Pearson, M. Pernía-Leal, A.M. Beltrán, Y. Fernandez-Afonso, J. M. De la Fuente, R. Franco, E. Pereira and M. L. García-Martín, *Pharmaceutics*, 2021, **13**, 416.